Eur. Phys. J. A (2020) 56:7
https://doi.org/10.1140/epja/s10050-019-00001-1

THE EUROPEAN PHYSICAL JOURNAL A

Regular Article - Theoretical Physics

Finite-size effects in heavy halo nuclei from effective field theory

E. Ryberg[1], **C. Forssén**[1,a], **D. R. Phillips**[2,3,4], **U. van Kolck**[5,6]

[1] Department of Physics, Chalmers University of Technology, 412 96 Gothenburg, Sweden
[2] Institute of Nuclear and Particle Physics and Department of Physics and Astronomy, Ohio University, Athens, OH 45701, USA
[3] Institut für Kernphysik, Technische Universität Darmstadt, 64289 Darmstadt, Germany
[4] ExtreMe Matter Institute EMMI, GSI Helmholtzzentrum für Schwerionenforschung GmbH, 64291 Darmstadt, Germany
[5] Institut de Physique Nucléaire, CNRS/IN2P3, Université Paris-Sud, Université Paris-Saclay, 91406 Orsay Cedex, France
[6] Department of Physics, University of Arizona, Tucson, AZ 85721, USA

Received: 3 May 2019 / Accepted: 30 October 2019 / Published online: 14 January 2020

Communicated by V. Somà

Abstract Halo/Cluster Effective Field Theory describes halo/cluster nuclei in an expansion in the small ratio of the size of the core(s) to the size of the system. Even in the point-particle limit, neutron-halo nuclei have a finite charge radius, because their center of mass does not coincide with their center of charge. This point-particle contribution decreases as $1/A_c$, where A_c is the mass number of the core, and diminishes in importance compared to other effects, e.g., the size of the core to which the neutrons are bound. Here we propose that for heavy cores the EFT expansion should account for the small factors of $1/A_c$. As a specific example, we discuss the implications of this organizational scheme for the inclusion of finite-size effects in expressions for the charge radii of halo nuclei. We show in particular that a short-range operator could be the dominant effect in the charge radius of one-neutron halos bound by a P-wave interaction. The point-particle contribution remains the leading piece of the charge radius for one-proton halos, and so Halo EFT has more predictive power in that case.

1 Introduction

Theoretical models of many-body systems usually treat the constituent particles as having no internal structure. This point-particle approximation is also used in cluster models, e.g., for the description of halo systems [1–4], even though one might encounter situations for which the core is rather large. Finite-size effects are included a posteriori, but can become significant for certain observables. As an example, the total charge radius is usually calculated by simply adding in quadrature [5] the charge radii of the constituents and the calculated point-particle radius; see e.g. the calculation of charge radii for neutron-rich helium isotopes in the Gamow Shell Model [6]. Instead, it would be useful to construct a framework in which finite-size effects can be included systematically.

Constituent-size effects can be accounted for in effective field theories (EFTs), where they appear through derivative interactions. For example, the nucleon charge radius (and, more generally, nucleon form factors) can be calculated [7] in Chiral Perturbation Theory (ChPT) in an expansion in powers of $k_\pi/M_{\rm QCD}$, where $k_\pi \sim 150$ MeV is a momentum scale associated with the lightest carrier of the nuclear force, the pion, and $M_{\rm QCD} \sim 1$ GeV is the characteristic mass scale of QCD. The relevant pion parameters are its mass and decay constant. Chiral EFT [8] is a generalization of ChPT to a typical nucleus, for which the binding energy per nucleon is $B/A \sim k_\pi^2/M_{\rm QCD}$ and the radius $R \sim A^{1/3}/k_\pi$. The nuclear charge radius includes the sum of the nucleons' radii plus many-body effects generated by internucleon interactions and currents [9]. We would like to have a similar framework for clusterized systems.

Clusterized systems, with much smaller energies and larger radii, are additionally characterized by scales beyond the pion scales. These nuclei can be viewed as a collection of valence nucleons orbiting around either no core (few-nucleon systems), one core (halo nuclei) or many cores (cluster nuclei). The cores themselves frequently—but not always—have properties of typical nuclei. The generic existence of such systems can be understood as a consequence of a fine-tuning in QCD, which introduces a lighter momentum scale $\aleph \sim 30$ MeV [10,11]. For such loosely bound systems we can devise EFTs that exploit the separation of scales without involving pions explicitly. In these EFTs one considers processes with typical momenta $k_{\rm lo}$, such that $k_{\rm lo} \ll k_{\rm hi}$,

[a] e-mail: christian.forssen@chalmers.se

where $k_{\rm hi} \lesssim k_\pi$ is a high-momentum scale. One then develops an expansion for observables in powers of $k_{\rm lo}/k_{\rm hi}$. The very lightest nuclei are dilute systems with no core, where the dominant (two- and three-nucleon) interactions are S-wave. The corresponding EFT is Pionless EFT, for which power counting is relatively well understood [8].

Halo/Cluster EFT, here labeled HEFT, was proposed as an EFT for systems with one [12,13] or more [14] cores and valence nucleons [15,16]. (See Ref. [17] for a recent review.) HEFT power counting is a generalization of the power counting for Pionless EFT allowing for dominant interactions in waves with non-vanishing angular momentum and for a breakdown scale $k_{\rm hi}$ estimated from the first excitation of the core and/or its size. In the first cases considered, ^{5,6}He [12,13,18–20], there is an alpha-particle core, and the neutron–alpha (n–α) interaction is mostly of P-wave nature, generating a near-threshold ^{5}He resonance. The α–α interaction, in turn, is obtained [14] from α–α scattering and the lowest ^{8}Be state. HEFT has since been extended to heavier cores and to proton halo systems [17]. In most of these cases the high scale $k_{\rm hi}$ in HEFT is associated with the size of the core, i.e. $k_{\rm hi} \sim 1/R_{\rm c}$. This means HEFT is an expansion in powers of $R_{\rm c}/R_{\rm halo}$, where $R_{\rm halo}$ is the unnaturally large size of the halo system.

The different contributions to the charge radius of a halo nucleus can then be organized in the HEFT expansion and the size of the effect due to the finite size of the core (and of the nucleon) estimated. We do that and thereby derive—for both S- and P-wave one-neutron halos—the charge-radius formula that is frequently used in nuclear theory. However, we also point out that there is, in principle, another expansion parameter present when HEFT is applied to systems with a relatively large number, $A_{\rm c}$, of core nucleons. To leading order in $1/A_{\rm c}$ the core is static, its recoil being small compared to nucleon recoil. Consequently the center of mass of a neutron halo coincides with its center of charge. Thus, whereas for light halos (e.g. ^{6}He) the difference between these two generates an important contribution to the charge radius [21], for heavier systems the corresponding effect goes to zero. Correctly assessing the impact of the finite size of the constituents on the charge radius requires keeping track of factors of $1/A_{\rm c}$.

Moreover, the charge radii of halo nuclei are affected by a short-range operator, which is subleading in $R_{\rm c}/R_{\rm halo}$ but leading in $1/A_{\rm c}$. We show that for one-neutron halos bound by a P-wave interaction (e.g. the excited state of ^{11}Be) this effect may be as important as the long-distance contributions to the halo's charge radius that have been previously computed in HEFT [22]. Similar considerations also apply to the form factors of two-neutron halos such as those discussed in Ref. [23]. They are not, however, as pressing for proton halos, where a finite charge radius will be generated by the photon coupling to the valence proton(s) even if the core is infinitely heavy.

This exemplifies the importance of keeping track—to the extent possible—of factors of $1/A_c$ in observables, rather than just counting powers of $k_{\rm lo}$. This is quite similar to the need to distinguish between relativistic corrections that are suppressed by powers of the inverse nucleon mass, $1/m_{\rm N}$, and other corrections that only carry powers of $1/k_{\rm hi}$ [24–26]. The significant difference between these two scales produces a hierarchy between effects that scale with the same power of $k_{\rm lo}$. Only once that hierarchy has been identified can the power counting be formulated in an efficient manner.

We isolate the $A_{\rm c}$ dependence that enters the charge radius through kinematic effects, i.e., because the nucleon–core mass ratio, $m_{\rm N}/m_{\rm c}$, is small. In contrast, we assume that all Lagrangian coefficients (LECs) scale with a power of $k_{\rm hi}$ that is solely determined by the naive engineering dimension of the operator they multiply, i.e., we use naive dimensional analysis with respect to $k_{\rm hi}$ and do not attach any additional $A_{\rm c}$ dependence to the LECs. It is true that $k_{\rm hi}$ is also $A_{\rm c}$ dependent, because $k_{\rm hi}$ will generically be of order the inverse core size, $1/R_{\rm c}$, and $R_{\rm c}$ can be taken to be $\propto A_{\rm c}^{1/3}$. But any additional accounting of the $A_{\rm c}$ dependence of short-distance physics in HEFT beyond this would require a more microscopic understanding of the $A_{\rm c}$ dependence of all the coefficients in the EFT. This could be achieved by matching HEFT to a microscopic calculation, but it could be argued that such matching goes beyond the EFT philosophy of writing down a theory that is independent of the short-distance physics. In contrast, the kinematic effects we identify here are universal, in the sense that they occur irrespective of the nature of the forces between the halo nucleons and the core(s).

Here we focus on the charge radius of single-neutron halo nuclei, where the point contribution is suppressed by $1/A_{\rm c}$ for the reason described above. But the presence of the heavy-core propagator is ubiquitous, so similar effects will affect other observables as well. For example, one expects the Born–Oppenheimer approximation to emerge in systems with multiple heavy cores and/or valence nucleons.

Our paper is structured as follows: In Sect. 2 we discuss the interplay between the various scales that are involved in an EFT for a halo system with a heavy core. We also discuss the low-energy scattering parameters for the nucleon–core system and introduce the charge radius in terms of the momentum expansion of the low-energy charge form factor. In Sect. 3 we derive the observable charge radius for S- and P-wave one-neutron-halo states. The power counting is exemplified by considering the charge radius for selected halo states. We summarize our findings in Sect. 4. An appendix discusses the corresponding results for proton halos, where considering factors of $1/A_{\rm c}$ does not lead to any change in the hierarchy of the various physical mechanisms that contribute to the charge radius.

2 Power counting

Once the relevant degrees of freedom are chosen, a model consists of a specific set of interactions among them. In contrast, with an EFT one considers the most general dynamics consistent with the known symmetries. It is crucial to organize the corresponding infinity of contributions to any observable according to their size ("power counting").

We are interested in a clusterized system where the size $R_{\rm halo} \sim 1/k_{\rm lo}$ of the system is sufficiently large that the constituents can be taken as point-like in a first approximation. This system might be probed with particles (photons, electrons, neutrinos, nucleons) of wavelength $\sim 1/k_{\rm lo}$ that cannot resolve the inner structure of the constituents. For simplicity we consider a few valence nucleons orbiting around a single core of radius $R_{\rm c}$ consisting of $A_{\rm c} \gg 1$ nucleons. The arguments below can be generalized straightforwardly to multiple-core systems.

The power counting of HEFT is based, like that of other EFTs, on the ratio of momentum scales, $k_{\rm lo}/k_{\rm hi} \ll 1$. The high-momentum scale $k_{\rm hi}$ is determined by physics not accounted for explicitly in HEFT. Since nuclei are bigger than nucleons we must have $k_{\rm hi} \lesssim 1/R_{\rm N} \sim k_\pi$, with $R_{\rm N}$ the size of a nucleon, which is generically set by pionic dynamics described by ChPT. But a more restrictive condition on $k_{\rm hi}$ arises from the requirement that details of the core are not resolved:

$$k_{\rm hi} \lesssim 1/R_{\rm c}. \tag{1}$$

Adopting the standard rule for the scaling of the nuclear size with $A_{\rm c}$ we then have $k_{\rm hi} \sim A_{\rm c}^{-1/3} k_\pi$, although we note that several of the cores considered up until now in HEFT are somewhat larger than this valley-of-stability lore indicates. If there exist low-lying excited states of the core, corresponding to a lower momentum scale than the inverse size of the core, the high-momentum scale needs to be adjusted accordingly, or else explicit degrees of freedom must be introduced for the low-lying excited states. One example of this is in the $^7{\rm Be}(p,\gamma)^8{\rm B}$ reaction, where the low-lying excited state of ^{7}Be must be included as an explicit degree of freedom in the HEFT if Eq. (1) is to prevail [27,28].

$k_{\rm hi}^{-1}$ can therefore be expected to increase for heavier systems, rendering finite-size effects more important. Meanwhile, $1/A_{\rm c}$ decreases and will generically be smaller than $k_{\rm lo}/k_{\rm hi}$. It introduces an additional expansion parameter. Explicit factors of $1/A_{\rm c} \ll 1$ enter through the core mass,

$$m_{\rm c} \approx A_{\rm c} m_{\rm N}, \tag{2}$$

where the average nucleon mass $m_{\rm N} \simeq 940$ MeV and we have neglected the effect of nuclear binding for the kinematic purposes we have in mind here.

In our non-relativistic theory approximate Galilean invariance guarantees that the interactions depend on the mass of the particles only in trivial ways that can be scaled out of the theory. Therefore all explicit occurrences of $1/A_{\rm c}$ are associated with the kinematics of the two-particle system, and once again, Galilean invariance means that they must be encoded in the halo's reduced mass,

$$m_{\rm R} = \frac{m_{\rm N} m_{\rm c}}{M_{\rm cN}} = m_{\rm N}\left(1 - \frac{1}{A_{\rm c}} + \cdots\right), \tag{3}$$

where

$$M_{\rm cN} = m_{\rm c} + m_{\rm N} \equiv \frac{m_{\rm N}}{f}, \tag{4}$$

is the total nucleon–core mass, with $f \simeq 1/(A_{\rm c}+1) \sim 1/A_{\rm c}$. Specifically, $m_{\rm R}$ has a fractional difference from $m_{\rm N}$ of $\approx 1/A_{\rm c}$, reflecting the extent to which the core is still dynamical in the (effective) one-body problem.

The large mismatch in masses evident in Eq. (2) means that the pertinent energy scale for the valence nucleon is the one-nucleon separation energy

$$B_{\rm s} \sim \frac{k_{\rm lo}^2}{2m_{\rm R}}, \tag{5}$$

which is much smaller than the binding energy of the core but much larger than the recoil energy of the core

$$E_{\rm c} \sim B_{\rm s}/A_{\rm c}. \tag{6}$$

For energies of the order of the typical nucleon energy, $E \sim B_{\rm s}$, nucleon recoil is a leading-order effect. Beyond leading order the ratio $k_{\rm lo}/m_{\rm N}$ occurs only in (small) relativistic corrections. In contrast, core recoil is suppressed by a factor of $1/A_{\rm c}$. Thus at leading order (LO) the core propagator is static, that is,

$$S_{\rm c}(E,\boldsymbol{p}) = \frac{1}{E - \frac{\boldsymbol{p}^2}{2m_{\rm c}} + i\varepsilon} \to S_{\rm c}^{\rm LO}(E) = \frac{1}{E + i\varepsilon}. \tag{7}$$

Thus, for low-order calculations one can simplify the procedure by using a static core, and including recoil effects perturbatively as higher-order corrections. Relativistic corrections that scale like $k_{\rm lo}/m_{\rm c}$ will be even smaller.

In addition to these kinematic factors of $1/A_{\rm c}$, there may be dependence on $A_{\rm c}$ coming through the interaction coefficients, or "low-energy constants" (LECs). As a trivial example, electromagnetic interactions add up constructively for protons and the corresponding LECs in general depend on the core charge $Z_{\rm c} = A_{\rm c} - N_{\rm c}$. It is not clear how to deal with this quantity a priori. In neutron halos, $Z_{\rm c}$ can be significantly smaller than $A_{\rm c}/2$, but this is not necessarily so for proton halos. We will keep factors of $Z_{\rm c}$ explicit and deal with them on a case-by-case basis.

Likewise, the LECs for strong interactions might in specific cases represent some constructive or destructive interference in the interactions of the valence nucleon with the core nucleons. One way to determine the $A_{\rm c}$ dependence of

these LECs is by matching HEFT to the ab initio solution of the same system with a more fundamental EFT [27–29], in a region where both EFTs are valid. Another way is to look at systematic trends in LECs fitted to data for different cores. In either case a manifestation of strong A_c dependence would be a particularly large or small LEC value with respect to the expected power of k_{hi}. Since there is no clear case at this point, below we limit ourselves to the kinematical factors arising from the core mass, although the counting of factors of $1/A_c$ could be improved later if needed.

2.1 Nucleon–core scattering

EFTs incorporate from the start the coupling to the continuum, so that most calculations of halo structure, including form factors, are intimately connected with nucleon–core scattering. A discussion of nucleon–core interactions is therefore necessary for the calculation of form factors, and we briefly review previous work on the subject here.

First we consider a halo system where the dominant nucleon–core interaction is S-wave. In this case, an EFT where all forces are of contact type reduces to the effective range expansion (ERE) [8,30]. One can think of the scattering length a_0 as what characterizes the size of the halo system, and the effective range r_0 (and higher ERE parameters) as reflecting the breakdown scale, namely the size of the core. The large size of the halo system is manifest in a large scattering length, while higher effective-range parameters are assumed to have sizes set by $1/k_{hi}$:

$$\begin{aligned} a_0 &\sim 1/k_{lo} \sim R_{halo}\,, \\ r_0 &\sim 1/k_{hi} \sim R_c. \end{aligned} \tag{8}$$

For an S-wave nucleon bound to the core with separation energy $B_{s0} > 0$, the nucleon–core T matrix has a pole at $k = i\gamma_0$ with

$$\gamma_0 \equiv \sqrt{2m_R B_{s0}} \sim k_{lo}. \tag{9}$$

The power counting for this system is almost identical to that of Pionless EFT for an S-wave bound state [8,30], which was adopted, for example, in the form-factor calculation of Ref. [22]. Note, however, that the suppression of the core recoil by Eq. (6) means that in LO the nucleon–core reduced mass that enters scattering is m_N; see Eq. (3).

Similar considerations apply to higher partial waves, but differences arise from the different renormalization: the more singular character of the interactions requires more LECs at any given order. For P-wave nucleon–core scattering, for example, both the scattering "length" a_1 and the effective "range" r_1 appear at LO [12,13] [1]. The mildest assumption [13] is that the effective range, just as for S-waves, is not fine tuned and directly reflects the breakdown scale,

$$r_1 \sim k_{hi} \sim 1/R_c. \tag{10}$$

In this case $r_1 k^2$ is larger than the unitarity term ik^3, and S-matrix poles of non-zero energy require a single fine tuning,

$$a_1 \sim 1/(k_{lo}^2 k_{hi}). \tag{11}$$

Assuming the higher ERE parameters still scale with k_{hi}, they are all subleading, and at LO there are two poles: depending on the sign of $a_1 r_1$, a resonance on the real axis or a real/virtual bound-state pair with binding momentum

$$\gamma_1 \equiv \sqrt{2m_R B_{s1}} \sim k_{lo}, \tag{12}$$

in terms of the separation energy $B_{s1} > 0$. Thus, again, $1/k_{lo}$ is related to the size of the halo system. At NLO the unitarity term needs to be included. If treated exactly, a third pole appears with momentum $\sim k_{hi}$, that is, outside the EFT. In the unlikely case where there are three low-energy poles in the low-energy region, the k_{hi} in Eqs. (10) and (11) should be replaced by k_{lo} [12].

Just as for S-waves, the assumption that no further powers of $1/A_c$ appear in the ERE parameters implies that the only change in power counting when treating $1/A_c$ as small is the extra expansion (3).

2.2 Charge form factor

The sizes of the halo system and its components are manifest not only in the ERE parameters but also in the charge form factor. The charge form factor is obtained as the matrix element of the zeroth component of the electromagnetic four-current, J^μ, according to

$$F_{ch}(\boldsymbol{Q}) = \frac{1}{eZ_h}\langle J^0\rangle = 1 - \frac{r_{ch}^2}{6}\boldsymbol{Q}^2 + \cdots\,, \tag{13}$$

where Z_h is the proton number of the halo nucleus and $\boldsymbol{Q}$ is the momentum transfer. A measure of the size of the nucleus is the charge radius r_{ch}. We now look at the power counting for the observable charge form factor of one-nucleon halo systems. The discussion here follows Ref. [22], but makes explicit the factors of $1/A_c$ that were not incorporated into the power counting there. We discuss contributions to the charge form factor in the point-like limit, due to the finite size of the constituents, and from additional two-body (short-range) contributions, as displayed in Fig. 1. More details and explicit examples will be presented in Sect. 3.

We start by discussing the point-like part, r_{pt}, which comes from the photon coupling to the charge of the constituents. The corresponding operators in the Lagrangian have the general form $\psi^\dagger A_0 \psi$ where ψ denotes either the core or the nucleon field and A_0 is the zeroth component of the photon four-vector field. The point-like contribution is kinemat-

[1] Note that the P-wave scattering length and effective range have dimensions of volume and momentum, respectively.

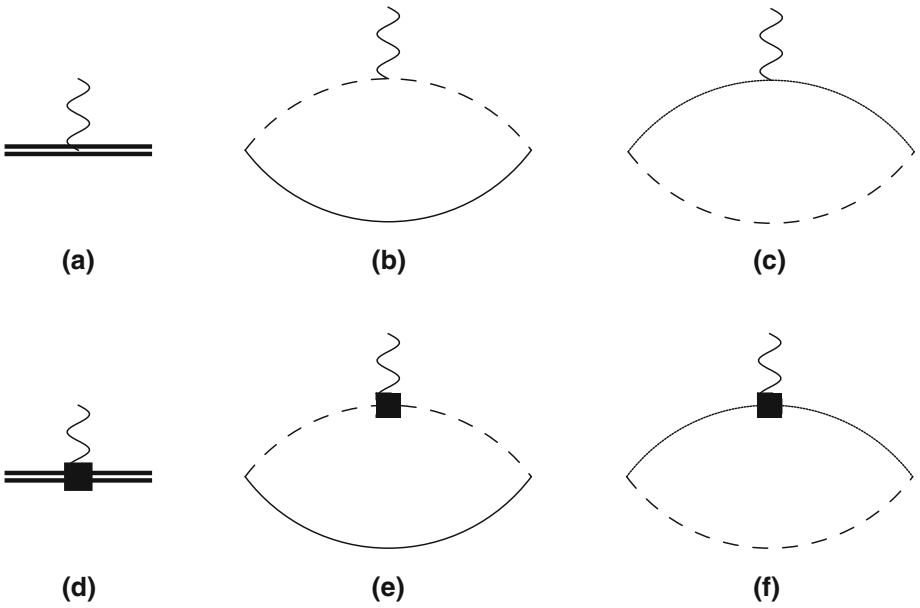

Fig. 1 Charge form-factor diagrams for a nucleon–core system. A solid/dashed/double/wavy line denotes a nucleon/core/dicluster/photon field. An unmarked (solid square) photon vertex is due to minimal (non-minimal) coupling, which is independent of (quadratic in) the photon momentum. The diagrams (**a**–**c**) give contributions to the point-like part of the charge radius. Diagrams (**d**–**f**) enter with the finite-size contribution of the core (**e**) and the nucleon (**f**), and through a short-range contribution (**d**)

ically generated by nucleon–core one-loop diagrams, where the photon couples to the core (in the neutron-halo case) or to both the core and the proton (for the proton halo)—see Fig. 1b, c. For a neutron halo, momentum dependence requires recoil of the core, and thus the charge radius, which involves two powers of momenta, is proportional to f^2, where f is defined in Eq. (4). Indeed, the loop for neutron-halo systems was calculated by Hammer and Phillips [22] with the leading-order (LO) results:

$$r^2_{\rm pt,LO} = \begin{cases} \frac{f^2}{2\gamma_0^2}\,, & \text{S-wave neutron halo,} \\ -\frac{5f^2}{2\gamma_1(3\gamma_1+r_1)}\,, & \text{P-wave neutron halo.} \end{cases} \tag{14}$$

The scalings are then given by

$$r^2_{\rm pt} \sim \begin{cases} 1/(A_{\rm c}^2 k_{\rm lo}^2)\,, & \text{S-wave neutron halo,} \\ 1/(A_{\rm c}^2 k_{\rm lo} k_{\rm hi})\,, & \text{P-wave neutron halo,} \end{cases} \tag{15}$$

assuming Eqs. (9), (10), and (12). However, it should be noted that typically $r_1 < 0$ so, if $|r_1|$ is close to $3\gamma_1$, then $|r_1 + 3\gamma_1|$ can in practice be $\sim k_{\rm lo}$ rather than the formally correct assignment $\sim k_{\rm hi}$ we have used here.

The point-like contribution to the charge radius is interesting because it can be calculated from known properties of the constituents, but it exists against a backdrop of other, less well-known contributions. One type of these other contributions comes from the finite sizes of the constituent core and nucleon, which enter through the same loop diagrams as the point contributions; see Fig. 1e, f. The finite-size contributions correspond to operators of the form $\psi^\dagger(\nabla^2 A_0)\psi$. The two extra powers of the small momentum compared to the point-like terms coming from minimal substitution means that, by naive dimensional analysis, this operator carries a suppression of $k_{\rm hi}^{-2}$. Such terms produce a direct contribution to the charge radius that is not suppressed by $A_{\rm c}^{-2}$. The nucleon finite-size contribution to $r^2_{\rm ch}$ will be denoted by $\rho^2_{\rm N}$ and should be proportional to $\rho^2_{\rm N} \sim R^2_{\rm N}$, i.e., to the proton or neutron charge radius squared, respectively, $\rho^2_{\rm p} = 0.766\ {\rm fm}^2$ [31] and $\rho^2_{\rm n} = -0.116\ {\rm fm}^2$ [32]. This contribution scales as

$$\rho^2_{\rm N}/Z_{\rm h} \sim R^2_{\rm N}/Z_{\rm h},\ \text{S-wave or P-wave halo.} \tag{16}$$

Meanwhile, the core-size contribution to the charge radius squared, $\rho^2_{\rm c}$, will scale as

$$\rho^2_{\rm c} \sim R^2_{\rm c} \sim 1/k^2_{\rm hi},\ \text{S-wave or P-wave halo.} \tag{17}$$

Taking the ratio of Eqs. (16) and (17) shows that in general the nucleon finite-size contribution to the charge radius squared is smaller than the core-finite-size contribution by both $(R_{\rm N}/R_{\rm c})^2$ and a factor of the total charge $Z_{\rm h}$ of the system. For the canonical estimate $R_{\rm c} \sim A_{\rm c}^{1/3} R_{\rm N}$ we have

$$\rho^2_{\rm N}/(Z_{\rm h}\rho^2_{\rm c}) \sim 1/(Z_{\rm h} A_{\rm c}^{2/3}). \tag{18}$$

There is another contribution to the charge radius, but this time it is not determined by data from other processes. Short-range contributions to the charge density are encoded in a contact operator of the form $\Psi^\dagger(\nabla^2 A_0)\Psi$, where Ψ denotes the dicluster field for either the S- or the P-wave system—see Fig. 1d. Because of the two derivatives, this operator is suppressed by a factor of $k_{\rm hi}^{-2}$ with respect to $\Psi^\dagger A_0 \Psi$, which originates in the minimal substitution of the dicluster kinetic term—Fig. 1a. The minimal substitution term ensures that the charge comes out correct; the term with two additional derivatives comes with short-range parameters, which we denote in S- and P-wave halos by, respectively, $\rho^2_{\sigma,\pi} \sim k_{\rm hi}^{-2}$. In the case of an S-wave halo, the dicluster kinetic term is itself a relative $k_{\rm hi}^{-1}$ effect (it gives rise to the range, Eq. (8)), for an overall $k_{\rm hi}^{-3}$ suppression. For a P-wave system, the dicluster

kinetic term leads to the "range" which scales with $k_{\rm hi}$; see Eq. (10), and there is no extra suppression [22]. We expect short-range contributions to the charge radius that scale as

$$\begin{cases} \gamma_0 r_0 \rho_\sigma^2 \sim k_{\rm lo}/k_{\rm hi}^3, & \text{S-wave halo,} \\ \rho_\pi^2 \sim 1/k_{\rm hi}^2, & \text{P-wave halo,} \end{cases} \tag{19}$$

again shown explicitly in Sect. 3. Thus, for S-wave one-nucleon halos this short-range operator enters one order after the core-size contribution. For P-wave halos both contribute at the same order.

In summary, these power-counting arguments make explicit that the point-like contribution for one-nucleon halos involves a kinematical suppression factor $1/A_{\rm c}^2$ for neutron halos. But this has the consequence that, for P-wave one-neutron halos, a short-range operator enters at the same order as the finite-size core contribution. The existence of such additional short-range operators will have negative influence on the predictive power of LO calculations.

3 The charge-radius formula

In this section we will derive charge-radius formulas in HEFT with the heavy-core power counting. In the process we will critique some results from Ref. [22] where finite-size effects were not treated explicitly. For example, the charge radius formula used in Ref. [22] for a one-neutron-halo system is

$$r_{\rm ch}^2 = r_{\rm pt}^2 + \rho_{\rm c}^2, \tag{20}$$

where $\rho_{\rm c}^2$ is the charge radius squared of the core. In principle, one should also add the neutron charge-radius contribution $\rho_{\rm n}^2/Z_{\rm c}$, where $Z_{\rm c}$ is the core charge, but this term is usually neglected since $|\rho_{\rm n}^2|$ is tiny. The key point is that Eq. (20) has not been derived within the field theory: finite-size contributions were instead added to the point-like result in a rather ad hoc fashion. In what follows we will show that $\rho_{\rm c}^2$ (and, for that matter, $\rho_{\rm n}^2/Z_{\rm c}$) indeed add to the charge radius squared, but in principle other contributions of similar size can appear. We also argue that it is important to keep track of the large suppression in neutron halos of the point-like radius for $A_{\rm c} \gg 1$, when the main contribution to the charge radius of the system comes from the finite size of the constituents.

This derivation, carried out in the next subsections, starts from the HEFT Lagrangian. We will consider explicitly only dominant S- or P-wave interactions, and a spin-0 core—generalizations are straightforward but cumbersome to write. The Lagrangian for a spin-1/2 nucleon N_s, where $s = -1/2, 1/2$, and a spin-0 core c with S- and P-wave interactions is given by

$$\begin{aligned} \mathcal{L} =& N_s^\dagger \Big[i\partial_0 - \frac{e}{2}(1+\tau_3)A_0 + \frac{\nabla^2}{2m_{\rm N}} - \frac{e}{12}\Big[\left(\rho_{\rm p}^2 + \rho_{\rm n}^2\right) \\ &+ \left(\rho_{\rm p}^2 - \rho_{\rm n}^2\right)\tau_3 \Big](\nabla^2 A_0) + \cdots \Big] N_s \\ &+ c^\dagger \Big[i\partial_0 - eZ_{\rm c}A_0 + \frac{\nabla^2}{2m_{\rm c}} - \frac{eZ_{\rm c}\rho_{\rm c}^2}{6}(\nabla^2 A_0) + \cdots \Big] c \\ &+ \sigma_s^\dagger \Big[\Delta_0 + \eta_0 \Big(i\partial_0 \\ &- eZ_{\rm h}A_0 + \frac{\nabla^2}{2M_{\rm cN}} - \frac{eZ_{\rm h}}{6}\rho_\sigma^2 (\nabla^2 A_0) \Big) + \cdots \Big] \sigma_s \\ &- g_0 \Big[\sigma_s^\dagger c N_s + \text{H.c.} \Big] + \cdots \\ &+ \pi_s^\dagger \Big[\Delta_1 + \eta_1 \Big(i\partial_0 - eZ_{\rm h}A_0 + \frac{\nabla^2}{2M_{\rm cN}} \\ &- \frac{eZ_{\rm h}}{6}\rho_\pi^2 (\nabla^2 A_0) \Big) + \cdots \Big] \pi_s \\ &- g_1 \Big[\mathcal{C}_{si}^{s'} \pi_{s'}^\dagger c \left(i(1-f)\overrightarrow{\nabla}_i - if\overleftarrow{\nabla}_i \right) N_s + \text{H.c.} \Big] + \cdots . \end{aligned} \tag{21}$$

The field σ_s is the spin-1/2 dicluster field, which we introduce for convenience. Its kinetic term has a sign η_0 and it has a residual mass Δ_0, which is a parameter to be fixed. The most important S-wave coupling of nucleon and core has strength g_0. For the P-wave interaction, corresponding to the last two terms, we have, for simplicity, included only the $J = 1/2$ channel, through a spin-1/2 dicluster field π_s and the Clebsch–Gordan coefficient $\mathcal{C}_{si}^{s'} = \left(\frac{1}{2}s1i\middle|\left(\frac{1}{2}1\right)\frac{1}{2}s'\right)$ [22]. The indices take values according to $s, s' = -1/2, 1/2$ and $i = -1, 0, 1$. As above, η_1 is a sign, and Δ_1 and g_1 are parameters to be fixed, while f was defined in Eq. (4). The field A_0 is the zeroth component of the photon four-vector field. Here τ_3 is the third isospin Pauli matrix, and we have defined the charge number of the core $Z_{\rm c}$. Note that $Z_{\rm h}$ is the charge ($Z_{\rm c}$ or $Z_{\rm c}+1$) of the nucleon–core system. The charge radius of the nucleon (core) field is $\rho_{\rm N}$ ($\rho_{\rm c}$), while ρ_σ and ρ_π are additional short-range parameters with sizes given by Eq. (19), which will be discussed below.

This Lagrangian includes all operators that will contribute to the charge radius of the halo system up to NLO. Higher-order terms, such as the one that leads to the shape parameter in the ERE and terms that do not contribute to the charge form factor, are denoted by the ellipsis. The coefficients of the $\nabla^2 A_0$ terms in Eq. (21) encode the finite size and composite nature of the core. We assign the same scaling to them as Hammer and Phillips, who used naive dimensional analysis to argue that $\rho_{\rm c}^2, \rho_\sigma^2, \rho_\pi^2$ are all $\sim R_{\rm c}^2$ [2]. However, whereas Ref. [22] argued that this scaling rendered these effects of higher order, here we contend that they can provide the main contribution to the charge radius for heavy-core systems.

[2] For ρ_π^2, which undergoes renormalization, this estimate is only valid for a renormalization scale of order $k_{\rm hi}$; see below.

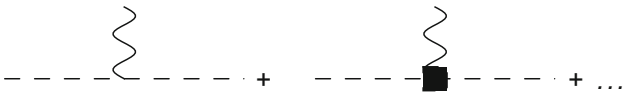

Fig. 2 Diagrams for the charge form factor of the core. The first diagram has a vertex ieZ_c and the second diagram gives the charge radius of the core, through the vertex $-ieZ_c\rho_c^2 Q^2/6$

The finite constituent sizes are reflected in the non-trivial momentum-transfer dependence of the core and nucleon form factors. The form factor of the core is given by the part of the Lagrangian where a photon couples to the core field, that is, terms of the form $c^\dagger A_0 c$ (and derivatives of A_0). The resulting charge form factor of the core is thus given by the diagrams shown in Fig. 2 as

$$F_{\mathrm{ch,c}}(\boldsymbol{Q}) = \frac{1}{eZ_c}\langle J_c^0\rangle = 1 - \frac{\rho_c^2}{6}\boldsymbol{Q}^2 + \cdots , \tag{22}$$

and as such the charge radius of the core is given by ρ_c. Note that since Fig. 2 contains no loops the Lagrangian parameter ρ_c^2 appears directly here without being affected by renormalization—at this order. The nucleon charge form factors and charge radii can be considered in a similar fashion, with the exception that the electric charge of the neutron is zero:

$$F_{\mathrm{ch,N}}(\boldsymbol{Q}) = \frac{1}{e}\langle J_N^0\rangle = Z_N - \frac{\rho_N^2}{6}\boldsymbol{Q}^2 + \cdots , \tag{23}$$

where $Z_N = 0\,(1)$ for the neutron (proton). We now examine the effect of these terms in the charge radii of S- and P-wave neutron halos, while the case of proton halos is discussed in the Appendix.

3.1 S-wave neutron halos

Here we compute the expectation value of the zeroth component of the electromagnetic current, $\langle J^0\rangle$, which appears in Eq. (13), for an S-wave one-neutron halo. The long-distance contributions to this quantity are well known, cf. Refs. [22,25,30], where the diagrams in Fig. 1a, b were evaluated (although only for $A_c = 1$ in Refs. [25,30]). Here we include diagrams Fig. 1d–f as well, and so account for finite-size effects and the leading short-range, two-body operator.

The charge form factor of an S-wave one-neutron halo can be computed from the amputated correlator of the σ_s field with one insertion of all possible couplings to an A_0 photon. The diagrams that contribute up to $\mathcal{O}((k_{\mathrm{lo}}/k_{\mathrm{hi}})^3)$ are shown in Fig. 1. We must also apply a wavefunction renormalization factor $\mathcal{Z}_0$, which defines the overlap of the field σ_s with the physical one-neutron-halo state. The contributions from tree and loop diagrams can then be separated, viz.

$$F_{\mathrm{ch}}(\boldsymbol{Q}) = \frac{1}{eZ_c}\left[\Gamma_{\mathrm{tree}}(\boldsymbol{Q}) + \Gamma_{\mathrm{loop}}(\boldsymbol{Q})\right]. \tag{24}$$

The wavefunction renormalization factor is [22,30]

$$\mathcal{Z}_0 = \frac{2\pi\gamma_0}{g_0^2 m_R^2}(1-\gamma_0 r_0)^{-1}, \text{ up to NLO}, \tag{25}$$

where we kept some higher-order terms as well by not expanding the $(1-\gamma_0 r_0)^{-1}$ ratio. Note that $\mathcal{Z}_0$ is finite to this order.

At $\boldsymbol{Q} = 0$ finite-size effects cannot play a role as the photon only "sees" the entire charge of the system. The leading contribution to the form factor at $\boldsymbol{Q} = 0$ is then from the loop diagram in Fig. 1b, where the virtual photon is attached to the core via its charge. This diagram also gives rise to subleading corrections to $F_{\mathrm{ch}}(\boldsymbol{Q})$: it generates the point contribution to the form factor, but away from $\boldsymbol{Q} = 0$, this is suppressed by $1/A_c^2$ and not as large as other effects once $A_c \gg 1$.

The most important such other effect is due to the loop diagram Fig. 1e, i.e., the coupling of the A_0 photon to the finite size of the core inside the loop. The contribution of this graph can be combined with the corresponding coupling for the neutron, Fig. 1f, to obtain the contribution stemming from the constituent form factors, Eqs. (22) and (23). The result can be expressed as a coordinate-space integral,

$$\begin{aligned}\Gamma_{\mathrm{loop}}(\boldsymbol{Q}) = eZ_c\frac{g_0^2 m_R^2}{2\pi}\mathcal{Z}_0\int \mathrm{d}r\mathrm{d}(\cos\theta)\exp(-2\gamma_0 r)\\ \times\left[\left(1-\frac{\rho_c^2}{6}\boldsymbol{Q}^2\right)\exp(if\,\boldsymbol{Q}\cdot\boldsymbol{r})\right.\\ \left.-\frac{\rho_n^2}{6Z_c}\boldsymbol{Q}^2\exp(i(1-f)\boldsymbol{Q}\cdot\boldsymbol{r})\right].\end{aligned} \tag{26}$$

We expand the integral (26) up to order $\boldsymbol{Q}^2$ to arrive at

$$\begin{aligned}\Gamma_{\mathrm{loop}}(\boldsymbol{Q}) = eZ_c\frac{g_0^2 m_R^2}{2\pi\gamma_0}\mathcal{Z}_0\\ \times\left[1-\left(\rho_c^2+\frac{\rho_n^2}{Z_c}+\frac{f^2}{2\gamma_0^2}\right)\frac{\boldsymbol{Q}^2}{6}+\cdots\right].\end{aligned} \tag{27}$$

At $\mathcal{O}(k_{\mathrm{lo}}/k_{\mathrm{hi}})$, $F_{\mathrm{ch}}(\boldsymbol{Q})$ also receives a contribution from the tree-level diagram, Fig. 1a. Considering also the $O((k_{\mathrm{lo}}/k_{\mathrm{hi}})^3)$ tree diagram in Fig. 1d, which represents the short-range contribution to the halo charge radius, we arrive at

$$\Gamma_{\mathrm{tree}}(\boldsymbol{Q}) = -eZ_c\frac{g_0^2 m_R^2}{2\pi r_0}\mathcal{Z}_0\left(1-\frac{\rho_\sigma^2}{6}\boldsymbol{Q}^2\right). \tag{28}$$

The first term here is a consequence of charge conservation and ensures that as $\boldsymbol{Q}\to 0$ we have $F_{\mathrm{ch}}(0) = 1$, that is, the charge form factor is correctly normalized at zero momentum transfer. Moving away from $\boldsymbol{Q}\to 0$ we insert Eqs. (28) and (27) in Eq. (24), and compare with the term quadratic in momentum in Eq. (13), to obtain the charge-radius formula for S-wave neutron halos,

Table 1 Orders of the various contributions to the charge radius of S-wave neutron halos listed in Eq. (30). In each column effects of a particular order in the usual HEFT expansion parameter $k_{\rm lo}/k_{\rm hi}$ appear. Meanwhile the rows organize contributions due to additional small factors: inverse powers of the number of core nucleons ($A_{\rm c}$) and protons ($Z_{\rm c}$)

	$\mathcal{O}(k_{\rm lo}^{-2})$	$\mathcal{O}((k_{\rm lo}k_{\rm hi})^{-1})$	$\mathcal{O}(k_{\rm hi}^{-2})$	$\mathcal{O}(k_{\rm lo}k_{\rm hi}^{-3})$
$\mathcal{O}(1)$	—	—	$\rho_{\rm c}^2$	$\gamma_0 r_0(\rho_{\rm c}^2-\rho_\sigma^2)$
$\mathcal{O}(A_{\rm c}^{-3/2}Z_{\rm c}^{-1})$	—	—	$\rho_{\rm n}^2/Z_{\rm c}$	$\gamma_0 r_0\,\rho_{\rm n}^2/Z_{\rm c}$
$\mathcal{O}(A_{\rm c}^{-2})$	$r_{\rm pt,LO}^2$	$\gamma_0 r_0\, r_{\rm pt,LO}^2$	$\cdots$	$\cdots$

$$r_{\rm ch}^2 = \frac{1}{1-\gamma_0 r_0}\left(r_{\rm pt,LO}^2+\rho_{\rm c}^2+\frac{\rho_{\rm n}^2}{Z_{\rm c}}-\gamma_0 r_0\rho_\sigma^2\right)+\cdots\,, \tag{29}$$

where the "$\cdots$" represent higher-order contributions. Note that at this order the Lagrangian parameter ρ_σ^2 appears directly here, without renormalization. This is because the LO loop that gives the point-charge contribution is finite. The point-charge contribution to $r_{\rm ch}^2$ was computed in Ref. [22] as $(1-\gamma_0 r_0)^{-1}r_{\rm pt,LO}^2$, with $r_{\rm pt,LO}^2$ given by Eq. (14).

Expanding in $\gamma_0 r_0$,

$$r_{\rm ch}^2 = \rho_{\rm c}^2+\gamma_0 r_0\left(\rho_{\rm c}^2-\rho_\sigma^2\right)+\cdots + \left(\frac{\rho_{\rm n}^2}{Z_{\rm c}}+r_{\rm pt,LO}^2\right)(1+\gamma_0 r_0+\cdots)\,, \tag{30}$$

where the orders of various contributions are summarized in Table 1, assuming that $R_{\rm N}/R_{\rm c}\lesssim A_{\rm c}^{-1/3}$. If $A_{\rm c}\sim 1$, the most important terms are given by the point-radius $r_{\rm pt,LO}^2$. For larger $A_{\rm c}$, these terms rapidly lose importance, as do contributions from the neutron size. Unless we are dealing with light halos, we expect the dominant contribution to the difference in charge radii between halo and core to be given by $\gamma_0 r_0(\rho_{\rm c}^2-\rho_\sigma^2)$. This is an example of a term that is missed if one simply adds the core radius by hand, rather than including it in the EFT as any other operator.

Unfortunately, while $\rho_{\rm c}$ can be extracted from the core form factor (22), ρ_σ is a short-range term that cannot easily be extracted from a quantity other than the halo form factor itself. Since this is a short-range effect it is possible that it can be efficiently extracted from ab initio calculations of the charge radius. In such a calculation the difference between ρ_σ and $\rho_{\rm c}$ can be viewed as originating in two effects:

1. A change in the size of the core when it is placed in the bound state with the neutron.
2. Pieces of the ab initio wave function not in the core + neutron piece of the Hilbert space, e.g., those due to excited states of the core.

These effects cannot, however, be separated in a model-independent way, and only their combination enters through $\rho_{\rm c}^2-\rho_\sigma^2$.

As a concrete example we consider the S-wave ground state of the one-neutron halo ^{11}Be, whose form factor and photodisintegration were investigated in Ref. [22]. The neutron separation energy is $B_{\rm s0}=0.502$ MeV [33], corresponding to $k_{\rm lo}\sim\gamma_0\simeq 30$ MeV through Eq. (9). Using the charge radius of the ^{10}Be core, $\rho_{\rm c}=2.357(18)$ fm [34], as an estimate for its size, the breakdown scale is $k_{\rm hi}\sim 1/R_{\rm c}\simeq 80$ MeV. This is also the momentum $\sqrt{2m_{\rm R}E_{\rm ex}}\simeq 80$ MeV $\sim k_{\rm hi}$ corresponding to the first excitation of the core at $E_{\rm ex}=3.368$ MeV [35], so there is no need to include a field for this state. These scales then give us the expansion parameter $k_{\rm lo}/k_{\rm hi}\approx 0.4$. This means that $r_{\rm pt,LO}^2$ is numerically of the same size as $\mathcal{O}((k_{\rm lo}/k_{\rm hi})^3)$ corrections. Since $Z_{\rm c}\sim A_{\rm c}k_{\rm lo}/k_{\rm hi}$, the neutron-radius contributions are suppressed by more than five powers of $k_{\rm lo}/k_{\rm hi}$ compared to $\rho_{\rm c}$. At LO there is a charge-radius prediction, but it is trivial since it is just the charge radius of the ^{10}Be core, $\rho_{\rm c}^2\simeq 5.56(4)$ fm^2. This does, though, explain most of the measured value of $r_{^{11}{\rm Be}}^2\simeq 6.07(8)$ fm^2 ($r_{^{11}{\rm Be}}=2.463(16)$ fm [34]). Estimating $\gamma_0 r_0$ from the EFT expansion parameter ~ 0.4, we find that the point-charge contribution to $r_{\rm ch}^2$, i.e., the first term of Eq. (29), is $r_{\rm pt,LO}^2/(1-\gamma_0 r_0)\simeq 0.3$ fm^2. This explains more than half of the difference $r_{^{11}{\rm Be}}^2-r_{^{10}{\rm Be}}^2$. The rest must come from the short-distance effect ρ_σ^2: the experimental value for $r_{^{11}{\rm Be}}$ can be reproduced if the short-range parameter is given by $\rho_\sigma^2\approx 5.1$ fm^2, which is of the expected order of magnitude, $1/k_{\rm hi}\sim 2.5$ fm. This supports the power counting presented here. We thus see that ρ_σ^2 must be a little smaller than $\rho_{\rm c}^2$ in order to explain the data, although the errors on the atomic measurements of the ^{10}Be and ^{11}Be radii make it difficult to extract a precise value for $\rho_{\rm c}^2-\rho_\sigma^2$.

3.2 P-wave neutron halos

An important aspect of the S-wave halo system is that all the charge form-factor diagrams we considered are finite. For P waves this is not the case. The increased singularity of the P-wave interaction can be seen already in the need for the effective-range term (10) at LO to allow proper renormalization of nucleon–core scattering. As before we will consider operators up to second order in the photon momentum $\boldsymbol{Q}$ and will show that, if the charge-radius contributions of the

constituents are to be considered explicitly, we need an additional short-range operator to renormalize the halo charge radius.

Since the cancelation of divergences will be critical to what follows we recapitulate the formulas for neutron–core scattering derived in Refs. [12,22]. The power counting discussed in Sect. 2.1 indicates that neutron–core scattering proceeds through the bare dicluster propagator at LO, and by an insertion of one nucleon–core bubble at NLO. Up to this order, elastic scattering with a P-wave interaction gives the matching

$$\frac{1}{a_1} = \frac{6\pi\Delta_1}{g_1^2 m_{\rm R}} + \frac{2L_3}{\pi}\,, \tag{31}$$

$$r_1 = -\frac{6\pi\eta_1}{g_1^2 m_{\rm R}^2} - \frac{4L_1}{\pi}\,, \tag{32}$$

where the $L_n = \int {\rm d}p\, p^{n-1}$ are divergent integrals in the irreducible dicluster self-energy,

$$\Sigma_1(E) = \frac{g_1^2 m_{\rm R}}{6\pi}\left[\frac{2L_3}{\pi} + \frac{4L_1}{\pi} m_{\rm R} E + i(2m_{\rm R}E)^{3/2}\right]. \tag{33}$$

It is evident from Eqs. (31) and (32) that two parameters, Δ_1 and g_1, are needed to renormalize scattering up to NLO. The P-wave wavefunction renormalization is given by

$$\mathcal{Z}_1 = -\frac{6\pi}{g_1^2 m_{\rm R}^2 r_1}\left(1 + \frac{3\gamma_1}{r_1}\right)^{-1}, \text{ up to NLO.} \tag{34}$$

Note that, contrary to the S-wave wavefunction renormalization (25), $\mathcal{Z}_1$ is not finite to this order.

The P-wave charge form-factor diagrams are similar to those for the S-wave interaction, Fig. 1. The tree diagrams amount to

$$\Gamma_{\rm tree}(\boldsymbol{Q}) = \eta_1 e Z_{\rm c} \mathcal{Z}_1 \left(1 - \frac{\rho_\pi^2}{6}\boldsymbol{Q}^2\right), \tag{35}$$

while the one-loop diagrams give

$$\begin{aligned}\Gamma_{\rm loop}(\boldsymbol{Q}) = {} & e Z_{\rm c} \frac{g_1^2 m_{\rm R}^2 \gamma_1^2}{6\pi} \mathcal{Z}_1 \int {\rm d}r {\rm d}(\cos\theta) \left(1 + \frac{1}{\gamma_1 r}\right)^2 \\ & \times \exp(-2\gamma_1 r)\left[\left(1 - \frac{\rho_{\rm c}^2}{6}\boldsymbol{Q}^2\right)\exp(if\,\boldsymbol{Q}\cdot\boldsymbol{r}) \right. \\ & \left. - \frac{\rho_{\rm n}^2}{6Z_{\rm c}}\boldsymbol{Q}^2 \exp(i(1-f)\,\boldsymbol{Q}\cdot\boldsymbol{r})\right].\end{aligned} \tag{36}$$

Expanding in powers of the momentum transfer $\boldsymbol{Q}$,

$$\begin{aligned}\Gamma_{\rm loop}(\boldsymbol{Q}) = {} & -e Z_{\rm c} \frac{g_1^2 m_{\rm R}^2 \gamma_1}{2\pi} \mathcal{Z}_1 \left\{\left(1 - \frac{4L_1}{3\pi\gamma_1}\right)\right. \\ & \left. \times \left[1 - \left(\rho_{\rm c}^2 + \frac{\rho_{\rm n}^2}{Z_{\rm c}}\right)\frac{\boldsymbol{Q}^2}{6}\right] + \frac{5f^2}{6\gamma_1^2}\frac{\boldsymbol{Q}^2}{6} + \cdots\right\}.\end{aligned} \tag{37}$$

The only difference with respect to the S-wave, apart from $\mathcal{Z}_1$, is that the P-wave bound-state wavefunction is $\left[1 + 1/(\gamma_1 r)\right]\exp(-\gamma_1 r)$, which is irregular at the origin. As a consequence, the integral that appears already in the momentum-independent term is divergent, and related to one of the divergent integrals in $\Sigma(E)$, the L_1 of Eq. (32).

The divergence in the momentum-independent contribution cancels between Eqs. (35) and (37), and we obtain a properly normalized form factor, $F_{\rm ch}(0) = 1$ [22]. The terms quadratic in momentum give the charge radius,

$$r_{\rm ch}^2 = r_{\rm pt,LO}^2 + \rho_{\rm c}^2 + \frac{\rho_{\rm n}^2}{Z_{\rm c}} + \bar{\rho}_\pi^2 + \cdots, \tag{38}$$

where the LO point-charge contribution, defined in Eq. (14), agrees with Ref. [22], and the (finite) short-range contribution $\bar{\rho}_\pi^2$ is related to the counterterm ρ_π^2 by

$$\bar{\rho}_\pi^2 = \frac{1}{r_1 + 3\gamma_1}\left(r_1 + \frac{4L_1}{\pi}\right)\left(\rho_\pi^2 - \rho_{\rm c}^2 - \frac{\rho_{\rm n}^2}{Z_{\rm c}}\right). \tag{39}$$

An interesting point here is that the finite contribution of $\rho_{\rm c}^2$ to $r_{\rm ch}^2$ from Eq. (37) is suppressed by an additional factor $\gamma_1/r_1 \sim k_{\rm lo}/k_{\rm hi}$ with respect to the estimate (17). The appearance of the full $\rho_{\rm c}^2$ in (38) is a consequence of the particular renormalization condition (39).

In this renormalization scheme the effect beyond the "standard" charge-radius formula depends on the extent to which the dicluster counterterm differs from the core radius. In contrast to the S-wave case, here the difference $\rho_\pi^2 - \rho_{\rm c}^2 - \rho_{\rm n}^2/Z_{\rm c}$ must go to zero as the regulator is taken to infinity, in order to yield a finite $\bar{\rho}_\pi^2$. It is important to consider what would happen if we were to include the finite-size contributions, but not the ρ_π^2 short-range operator. In Eq. (37) we see that the constituent charge radii enter with a prefactor that corresponds to a divergent integral. Since the parameters $\rho_{\rm c}^2$ and $\rho_{\rm n}^2$ are observables—these are the charge radii of the core and the neutron—they cannot absorb this divergence. The only parameter available for this purpose is the ρ_π^2. As such it is not possible to add the finite-size contributions without also including the short-range operator. Formally, the scaling of ρ_π^2 is $\rho_\pi^2 \sim \bar{\rho}_\pi^2 \sim R_{\rm c}^2$ for renormalization scales such that $L_1 \sim k_{\rm hi}$. However, the crucial difference between ρ_π^2 and $\bar{\rho}_\pi^2$ is that the latter is an observable, while the former absorbs a divergence and so is scheme- and regulator-dependent.

As an explicit example, let us consider the P-wave excited state of ^{11}Be with neutron separation energy $B_{\rm s1} = 0.182$ MeV [33]. The breakdown scale for this EFT was argued in Sect. 3.1 to be $k_{\rm hi} \sim 80$ MeV. These scales then give us the expansion parameter $k_{\rm lo}/k_{\rm hi} \approx 0.2$ for the P-wave system. The corresponding charge-radius formula is simply organized as

$$r_{^{11}{\rm Be}^*}^2 = \underbrace{\rho_{\rm c}^2 + \bar{\rho}_\pi^2}_{1/k_{\rm hi}^2} + \cdots + \underbrace{\left[r_{\rm pt,LO}^2 + \cdots\right]}_{1/(k_{\rm lo}k_{\rm hi})\times 1/A_{\rm c}^2} + \cdots \tag{40}$$

In this case, the LO result is given by the combination of the charge radius of ^{10}Be and an undetermined short-range parameter. The dots refer to corrections due to non-included interactions and the finite neutron size. We show the point-charge contribution explicitly to emphasize that it appears at N^{2}LO in the heavy-core power counting. This means that the charge radius for the P-wave state in ^{11}Be cannot be predicted in HEFT using the heavy-core power counting, unless the short-range parameter can be fixed to some other observable.

4 Conclusion

HEFT offers a systematic approach to make model-independent predictions of low-energy observables. In this paper we have discussed a new power-counting scheme for systems with a heavy-core nucleus, and we have derived the finite-size contributions to charge radii of one-nucleon halos. HEFT in general is restricted by appearances of short-range operators at rather low orders. With the heavy-core power counting, these restrictions are even enhanced for some systems and observables. For one-neutron halos where the core is much heavier than the neutron, the point-particle result for the charge radius is demoted from leading to subleading order since the core recoil due to the photon interaction is very small. In contrast, in the case of an S-wave system, the LO charge radius is given by the finite-size contributions of the constituents. For a P-wave one-neutron halo the heavy-core version of HEFT is non-predictive at LO, since the LO charge radius includes an undetermined short-range operator [3].

Note, however, that not all systems are made less predictive in the heavy-core power counting. For proton halos there are no issues for the charge-radius results due to the core being heavy (as shown in the appendix). This is due to the fact that the photon also couples to the proton field, which has a larger recoil than the core field. Furthermore, the expectation for the future is that more cluster data will become available and that this data can then be used to fix the parameters of the corresponding HEFT.

While we considered in detail the case of one-nucleon halo charge radii, the suppression of some contributions by factors of the inverse of the number of core nucleons is not restricted to this class of observables. The suppression for radii can be traced to the small recoil of the core or, equivalently, to the fact that the heavy-core propagator is static at leading order. Similar effects will in principle be present in any calculation at the loop level, where the propagator appears, for example the structure (energies, form factors, etc.) of two-nucleon halos or two-core systems. We leave the investigation of these additional implications of heavy cores to the future.

Acknowledgements Open access funding provided by Chalmers University of Technology. DRP and UvK acknowledge the hospitality of Chalmers University of Technology where this research was initiated. DRP thanks W. Elkamhawy for useful discussion. ER and CF were supported by the European Research Council under the European Community's Seventh Framework Programme (FP7/2007–2013)/ERC grant agreement no. 240603, by the Swedish Foundation for International Cooperation in Research and Higher Education (STINT, IG2012-5158), and by the Swedish Research Council (dnr. 2010-4078). The work of DRP was supported by the US Department of Energy under contract DE-FG02-93ER-40756 and by the ExtreMe Matter Institute EMMI at the GSI Helmholtzzentrum für Schwerionenphysik, Darmstadt, Germany. UvK's research was supported in part by the U.S. Department of Energy, Office of Science, Office of Nuclear Physics, under Award Number DE-FG02-04ER41338, and by the European Union Research and Innovation program Horizon 2020 under grant agreement no. 654002.

Data Availability Statement This manuscript has no associated data or the data will not be deposited. [Authors' comment: The manuscript has no associated data, as all calculations are fully explained and justified in the text.]

A Single-proton halos

For proton halos one needs additionally to account for Coulomb effects. Denoting by Z_c the charge of the core and by $\alpha = e^2/(4\pi)$ the fine-structure constant, the strength of the Coulomb interaction is characterized by the momentum scale $k_C \equiv Z_c \alpha m_R$. At energy E the relative importance of Coulomb is given by the Sommerfeld parameter $\eta \equiv k_C/\sqrt{2m_R E}$. For moderate Z_c, as in light nuclei, we expect $k_C \lesssim k_{lo}$. As Z_c increases the Coulomb force experienced by the halo proton increases. In that case, it might be appropriate to consider the limit $k_{lo}/k_C \ll 1$. The effects of Coulomb in proton halo systems have been examined in Refs. [28,37–42].

The charge form factor for proton halos involves the coupling of the photon to both the core and the proton. The point-like contribution to the charge radius is therefore not kinematically suppressed by $1/A_c^2$ and the scalings are naively

[3] As we were finalizing this manuscript we found that a similar conclusion has been reached by Elkamhawy and Hammer [36].

given by

$$r_{\rm pt}^2 \sim \begin{cases} 1/k_{\rm lo}^2\,, & \text{S-wave proton halo,} \\ 1/(k_{\rm lo}k_{\rm hi})\,, & \text{P-wave proton halo.} \end{cases} \tag{A.1}$$

These naive scalings are only valid if the Coulomb momentum is a low-momentum scale, that is, $k_{\rm C} \lesssim k_{\rm lo}$. If instead we are in the strong Coulomb regime, $k_{\rm C} \gg k_{\rm lo}$, the predictive power of LO calculations is reduced, which has been analyzed for S-wave one-proton halo states in Ref. [41,42]. For example, the point-like contribution for S-waves scales as $r_{\rm pt} \sim 1/k_{\rm C}$ if $k_{\rm C} \gg k_{\rm lo}$, which implies that the point-like contribution becomes suppressed by the strong Coulomb repulsion.

A.1 S-wave proton halos

The procedure for deriving the charge-radius formula for S-wave proton halos is similar to the neutron case; see Refs. [38,41]. However, there are four main differences:

(i) The total charge of the system is $Z_{\rm c}+1$.
(ii) The Coulomb interaction enters proton-core scattering and the wavefunction renormalization is given by

$$\mathcal{Z}_0 = \frac{6\pi k_{\rm C}}{g_0^2 m_{\rm R}^2} \times \begin{cases} \left(\frac{6k_{\rm C}^2}{m_{\rm R}}\frac{{\rm d}h_0(\eta)}{{\rm d}E}\right)^{-1}\Big|_{E=-B_{\rm s0}}, & \text{LO,} \\ \left(\frac{6k_{\rm C}^2}{m_{\rm R}}\frac{{\rm d}h_0(\eta)}{{\rm d}E} - 3k_{\rm C}r_0\right)^{-1}\Big|_{E=-B_{\rm s0}}, & \text{NLO,} \end{cases} \tag{A.2}$$

where

$$h_0(\eta) = \psi(i\eta) + \frac{1}{2i\eta} - \log(i\eta), \tag{A.3}$$

with ψ being the polygamma function. For $k_{\rm C} \gg \gamma_0$,

$$\frac{6k_{\rm C}^2}{m_{\rm R}}\frac{{\rm d}h_0(\eta)}{{\rm d}E} = 1 + \mathcal{O}\left(\frac{\gamma_0^2}{k_{\rm C}^2}\right). \tag{A.4}$$

As before, some higher-order terms are kept at NLO in Eq. (A.2).
(iii) The photon couples also to the proton in the proton–core loop of Fig. 1c, according to Eq. (23).
(iv) Coulomb interactions enter the loops in Fig. 1. The bound-state wavefunction is the Whittaker W-function $W_{-k_{\rm C}/\gamma_0,1/2}(2\gamma_0 r)$ instead of the exponential $\exp(-\gamma_0 r)$.

Taking these differences into account, the resulting charge-radius formula for an S-wave proton halo system is

$$r_{\rm ch}^2 = \left(\frac{6k_{\rm C}^2}{m_{\rm R}}\frac{{\rm d}h_0(\eta)}{{\rm d}E} - 3k_{\rm C}r_0\right)^{-1}\Big|_{E=-B_{\rm s0}} \times \left[r_{\rm pt,LO}^2 + \frac{Z_{\rm c}\rho_{\rm c}^2 + \rho_{\rm p}^2}{Z_{\rm c}+1} - 3k_{\rm C}r_0\rho_\sigma^2\right] + \cdots\,. \tag{A.5}$$

The leading-order point-charge contribution without the effective-range correction is given by

$$r_{\rm pt,LO}^2 = \frac{6\pi k_{\rm C}}{g_0^2 m_{\rm R}^2}\frac{\Gamma''_{\rm loop}(0)}{2e(Z_{\rm c}+1)}\,, \tag{A.6}$$

where the loop diagram is given in Ref. [41] as

$$\Gamma_{\rm loop}(\boldsymbol{Q}) = -eZ_{\rm c}\frac{g_0^2 m_{\rm R}^2}{8\pi^4}\,\Gamma(1+k_{\rm C}/\gamma_0)^2 \times \int {\rm d}r\; j_0(fQr)\; W_{-k_{\rm C}/\gamma_0,1/2}(2\gamma_0 r)^2 + [(f\to 1-f)\,,\ (Z_{\rm c}\to 1)]\,, \tag{A.7}$$

where j_0 is a spherical Bessel function of the first kind.

The $1/2^+$ excited state of ^{17}F was considered in HEFT by Ryberg et al. [38,41]. The $1/2^+$ excited state is located at 0.105 MeV below threshold [43], which then defines the low-momentum scale $k_{\rm lo} \sim 14$ MeV. The first excitation of the ^{16}O core is at about 6 MeV [43], so the size of the core defines the breakdown scale $k_{\rm hi}$ of about $1/R_{\rm c} \sim 60$–70 MeV, giving an expansion parameter $k_{\rm lo}/k_{\rm hi} \sim 0.2$. However, for the ^{16}O–proton system the Coulomb momentum scale $k_{\rm C} = 51.2$ MeV is much larger than the low-momentum scale and $3k_{\rm C}r_0$ is very close to unity [41]. This makes the effective-range prefactor in Eq. (A.5) very large, so this proton halo state cannot be well described without the inclusion of effective-range corrections. In practice, the ρ_σ^2 counterterm then enters at the same order as the finite-size contributions. Furthermore, in this strong Coulomb regime the LO point-like charge-radius contribution, $r_{\rm pt,LO}$, scales with $1/k_{\rm C}$, as was discussed in Ref. [41]. Therefore, organizing the charge-radius formula for the S-wave proton halo at hand, we have

$$r_{^{17}{\rm F}^*}^2 = \frac{1}{1-3k_{\rm C}r_0}\Big[\underbrace{r_{\rm pt,LO}^2}_{1/k_{\rm C}^2} + \underbrace{\frac{Z_{\rm c}}{Z_{\rm c}+1}\rho_{\rm c}^2 - 3k_{\rm C}r_0\rho_\sigma^2}_{1/k_{\rm hi}^2}\Big] + \cdots\,, \tag{A.8}$$

since $3k_{\rm C}r_0 \sim 1$ and $k_{\rm C} \gg \gamma_0$ for ^{17}F*.

The point-like contribution to the charge radius of ^{17}F*, including the finite-range correction, was evaluated by Ryberg et al. [41] to $r_{\rm pt,LO}^2/(1-3k_{\rm C}r_0) = (2.20 \pm 0.11\ {\rm fm})^2$. Here, the assigned uncertainty originates from the asymptotic normalization coefficient (ANC) obtained from a fit to

proton radiative-capture on ^{16}O. One should note that corrections from finite-size contributions and the short-range operator can be as large as $k_C/k_{hi} \approx 70\%$, unless at least parts of those corrections can be resummed. But Eq. (A.8) means that—at least formally—one may not add the finite-size contributions to the charge-radius result of ^{17}F* without also including the unknown short-range parameter ρ_σ^2.

A.2 P-wave proton halos

As for the S-wave proton halos, many of the details in the derivation of charge-radius formula for a P-wave proton halo are the same as for the P-wave neutron halo. Again, the differences are that the photon couples also to the proton, the bound-state wavefunctions are Whittaker W-functions, the total charge is $Z_c + 1$ and the wavefunction renormalization is now given by

$$\mathcal{Z}_1 = \frac{6\pi}{g_1^2 m_R^2}\left(r_1 - \frac{2k_C}{m_R}\frac{\mathrm{d}}{\mathrm{d}E}h_1(\eta)\right)^{-1}\Bigg|_{E=-B_{s1}}, \tag{A.9}$$

with $h_1(\eta) = p^2(1+\eta^2)h_0(\eta)$. For details, see Refs. [28,39]. The resulting charge-radius formula for a P-wave proton halo system is

$$r_{ch}^2 = \underbrace{r_{pt,LO}^2}_{1/(k_{lo}k_{hi})} + \underbrace{\frac{Z_c}{Z_c+1}\rho_c^2 + \bar{\rho}_\pi^2}_{1/k_{hi}^2} + \cdots, \tag{A.10}$$

where $\bar{\rho}_\pi^2$ is the renormalized short-range parameter. Here we emphasize the contribution $r_{pt,LO}^2$ is not kinematically suppressed for systems where both constituents are charged, since the photon couples through minimal substitution also to the proton. Therefore, if $\bar{\rho}_\pi^2$ is subleading to $r_{pt,LO}^2$, it is possible to give a low-order charge-radius prediction of P-wave proton halos without including the short-range parameter $\bar{\rho}_\pi^2$.

The point-charge contribution $r_{pt,LO}^2$ was derived in Ref. [39] and it is given by

$$r_{pt,LO}^2 = -\frac{3\mathcal{Z}_1}{e(Z_c+1)}\Gamma''_{loop}(0), \tag{A.11}$$

with the loop diagram given by

$$\begin{aligned}\Gamma_{loop}(Q) = &-\frac{e(Z_c+1)g_1^2 m_R^2 \Gamma(2+k_C/\gamma_1)^2\gamma_1^2}{3\pi}\\ &\times\int \mathrm{d}r\left[1-\left((1-f)^2+Z_c f^2\right)\frac{r^2Q^2}{6(Z_c+1)}\right.\\ &\left.+\mathcal{O}\left(Q^4\right)\right]\\ &\times W_{-k_C/\gamma_1,3/2}(2\gamma_1 r)^2.\end{aligned} \tag{A.12}$$

The one-proton separation energy of ^{8}B is $B_{s1} \simeq 0.138$ MeV [35], giving a low-momentum scale $k_{lo} \sim 15$ MeV. The ^{7}Be core has two low-lying states that were both included explicitly into the field theory: the $3/2^-$ ground state and the $1/2^-$ excited state at 0.429 MeV [44]. It can be argued that the breakdown scale for the EFT is given by the alpha-particle threshold at a momentum scale of $k_\alpha \simeq 51$ MeV [44] and thus the expansion parameter is about $k_{lo}/k_{hi} \sim 0.3$, or even as large as $k_C/k_{hi} \sim 0.5$ with $k_C = 23.8$ MeV.

The leading-order contribution to the charge radius of ^{8}B was evaluated by Ryberg et al. [39] to $r_{pt,LO}^2 = (2.56 \pm 0.08\ \mathrm{fm})^2$. Again, the uncertainty estimate comes from the relevant ANCs, which in this case were adopted from a microscopic ab initio computation by Nollett and Wiringa [45]. Alternatively, one can obtain the ANCs from a fit to proton radiative-capture $^7\mathrm{Be}(p,\gamma)^8B$. Such a fit was performed by Zhang et al. [28] and the ANCs are very consistent with the computed ones. However, the large expansion parameter suggests the finite-size and (unknown) short-range contributions to the charge radius of ^{8}B can be significant.

References

1. M.V. Zhukov, B.V. Danilin, D.V. Fedorov, J.M. Bang, I.J. Thompson, J.S. Vaagen, Bound state properties of Borromean Halo nuclei: He-6 and Li-11. Phys. Rept. **231**, 151–199 (1993). https://doi.org/10.1016/0370-1573(93)90141-Y
2. P.G. Hansen, A.S. Jensen, B. Jonson, Nuclear halos. Ann. Rev. Nucl. Part. Sci. **45**, 591–634 (1995). https://doi.org/10.1146/annurev.ns.45.120195.003111
3. A.S. Jensen, K. Riisager, D.V. Fedorov, E. Garrido, Structure and reactions of quantum halos. Rev. Mod. Phys. **76**, 215–261 (2004). https://doi.org/10.1103/RevModPhys.76.215
4. T. Frederico, A. Delfino, L. Tomio, M.T. Yamashita, Universal aspects of light halo nuclei. Prog. Part. Nucl. Phys. **67**, 939–994 (2012). https://doi.org/10.1016/j.ppnp.2012.06.001
5. J.L. Friar, J.W. Negele, Theoretical and Experimental Determination of Nuclear Charge Distributions. Adv. Nucl. Phys. **8**, 219–376 (1975)
6. G. Papadimitriou, A.T. Kruppa, N. Michel, W. Nazarewicz, M. Płoszajczak, J. Rotureau, Charge radii and neutron correlations in helium halo nuclei. Phys. Rev. C **84**, 051304 (2011). https://doi.org/10.1103/PhysRevC.84.051304. arXiv:1109.0223
7. V. Bernard, N. Kaiser, U.-G. Meißner, Chiral dynamics in nucleons and nuclei. Int. J. Mod. Phys. E **4**, 193–346 (1995). https://doi.org/10.1142/S0218301395000092. arXiv:hep-ph/9501384
8. P.F. Bedaque, U. van Kolck, Effective field theory for few nucleon systems. Ann. Rev. Nucl. Part. Sci. **52**, 339–396 (2002). https://doi.org/10.1146/annurev.nucl.52.050102.090637. arXiv:nucl-th/0203055
9. D.R. Phillips, Electromagnetic Structure of Two- and Three-Nucleon Systems: An Effective Field Theory Description. Ann. Rev. Nucl. Part. Sci. **66**, 421–447 (2016). https://doi.org/10.1146/annurev-nucl-102014-022321
10. S.R. Beane, P.F. Bedaque, M.J. Savage, U. van Kolck, Towards a perturbative theory of nuclear forces. Nucl. Phys. A **700**, 377–402 (2002). https://doi.org/10.1016/S0375-9474(01)01324-0. arXiv:nucl-th/0104030
11. U. van Kolck, Nuclear Physics from QCD. PoS Confinement **8**, 030 (2008). https://doi.org/10.22323/1.077.0030. arXiv:0812.3926

12. C.A. Bertulani, H.-W. Hammer, U. van Kolck, Effective field theory for halo nuclei. Nucl. Phys. A **712**, 37–58 (2002). https://doi.org/10.1016/S0375-9474(02)01270-8. arXiv:nucl-th/0205063
13. P.F. Bedaque, H.-W. Hammer, U. van Kolck, Narrow resonances in effective field theory. Phys. Lett. B **569**, 159–167 (2003). https://doi.org/10.1016/j.physletb.2003.07.049. arXiv:nucl-th/0304007
14. R. Higa, H.-W. Hammer, U. van Kolck, alpha alpha Scattering in Halo Effective Field Theory. Nucl. Phys. A **809**, 171–188 (2008). https://doi.org/10.1016/j.nuclphysa.2008.06.003. arxiv:0802.3426
15. D.L. Canham, H.-W. Hammer, Universal properties and structure of halo nuclei. Eur. Phys. J. A **37**, 367–380 (2008). https://doi.org/10.1140/epja/i2008-10632-4. arXiv:0807.3258
16. D.L. Canham, H.-W. Hammer, Range corrections for two-neutron halo nuclei in effective theory. Nucl. Phys. A **836**, 275–292 (2010). https://doi.org/10.1016/j.nuclphysa.2010.02.014. arXiv:0911.3238
17. H.-W. Hammer, C. Ji, D.R. Phillips, Effective field theory description of halo nuclei. J. Phys. **G44**(10), 103002 (2017). https://doi.org/10.1088/1361-6471/aa83db. arXiv:1702.08605
18. J. Rotureau, U. van Kolck, Effective Field Theory and the Gamow Shell Model: The ^{6}He Halo Nucleus. Few Body Syst. **54**, 725–735 (2013). https://doi.org/10.1007/s00601-012-0455-6. arXiv:1201.3351
19. C. Ji, C. Elster, D.R. Phillips, ^{6}He nucleus in halo effective field theory. Phys. Rev. C **90**(4), 044004 (2014). https://doi.org/10.1103/PhysRevC.90.044004. arXiv:1405.2394
20. E. Ryberg, C. Forssén, L. Platter, Three-body halo states in effective field theory: renormalization and three-body interactions in the helium-6 system. Few Body Syst. **58**(4), 143 (2017). https://doi.org/10.1007/s00601-017-1307-1. arXiv:1701.08576
21. Z.T. Lu, P. Mueller, G.W.F. Drake, W. Nörtershäuser, S.C. Pieper, Z.C. Yan, Colloquium: laser probing of neutron-rich nuclei in light atoms. Rev. Mod. Phys. **85**(4), 1383–1400 (2013). https://doi.org/10.1103/RevModPhys.85.1383. arXiv:1307.2872
22. H.-W. Hammer, D.R. Phillips, Electric properties of the Beryllium-11 system in Halo EFT. Nucl. Phys. A **865**, 17–42 (2011)
23. J. Vanasse, Charge and Matter Form Factors of Two-Neutron Halo Nuclei in Halo Effective Field Theory at Next-to-leading-order. arXiv:1609.08552
24. U. van Kolck, Effective field theory of short range forces. Nucl. Phys. A **645**, 273–302 (1999). https://doi.org/10.1016/S0375-9474(98)00612-5. arXiv:nucl-th/9808007
25. J.-W. Chen, G. Rupak, M.J. Savage, Nucleon-nucleon effective field theory without pions. Nucl. Phys. A **653**, 386–412 (1999). https://doi.org/10.1016/S0375-9474(99)00298-5. arXiv:nucl-th/9902056
26. X. Zhang, K.M. Nollett, D.R. Phillips, Models, measurements, and effective field theory: Proton capture on ^{7}Be at next-to-leading order. Phys. Rev. C **98**(3), 034616 (2018). https://doi.org/10.1103/PhysRevC.98.034616. arXiv:1708.04017
27. X. Zhang, K.M. Nollett, D.R. Phillips, Marrying ab initio calculations and Halo-EFT: the case of $^{7}\mathrm{Li} + n \rightarrow {}^{8}\mathrm{Li} + \gamma$. Phys. Rev. C **89**(2), 024613 (2014). https://doi.org/10.1103/PhysRevC.89.024613. arXiv:1311.6822
28. X. Zhang, K.M. Nollett, D.R. Phillips, Combining ab initio calculations and low-energy effective field theory for halo nuclear systems: the case of $^{7}Be + p \rightarrow {}^{8}B + \gamma$. Phys. Rev. C **89**(5), 051602 (2014). https://doi.org/10.1103/PhysRevC.89.051602. arXiv:1401.4482
29. G. Hagen, P. Hagen, H.-W. Hammer, L. Platter, Efimov Physics Around the Neutron-Rich ^{60}Ca Isotope. Phys. Rev. Lett. **111**(13), 132501 (2013). https://doi.org/10.1103/PhysRevLett.111.132501. arXiv:1306.3661
30. S.R. Beane, P.F. Bedaque, W.C. Haxton, D.R. Phillips, M.J. Savage, From hadrons to nuclei: Crossing the border 133–269 (2000). https://doi.org/10.1142/9789812810458_0011. arXiv:nucl-th/0008064
31. P.J. Mohr, D.B. Newell, B.N. Taylor, CODATA recommended values of the fundamental physical constants **2014**, (2015). https://doi.org/10.5281/zenodo.22826
32. K.A. Olive, Review of Particle Physics. Chin. Phys. C **40**(10), 100001 (2016). https://doi.org/10.1088/1674-1137/40/10/100001
33. F. Ajzenberg-Selove, Energy levels of light nuclei A = 11–12. Nucl. Phys. A **506**, 1–158 (1990). https://doi.org/10.1016/0375-9474(90)90271-M
34. W. Nörtershäuser, D. Tiedemann, M. Žáková, Z. Andjelkovic, K. Blaum, M.L. Bissell, R. Cazan, G.W.F. Drake, C. Geppert, M. Kowalska, J. Krämer, A. Krieger, R. Neugart, R. Sánchez, F. Schmidt-Kaler, Z.-C. Yan, D.T. Yordanov, C. Zimmermann, Nuclear charge radii of ^{7,9,10}Be and the one-neutron halo nucleus ^{11}Be. Phys. Rev. Lett. **102**, 062503 (2009). https://doi.org/10.1103/PhysRevLett.102.062503. http://link.aps.org/doi/10.1103/PhysRevLett.102.062503
35. D. Tilley, J. Kelley, J. Godwin, D. Millener, J. Purcell, C. Sheu, H. Weller, Energy levels of light nuclei a=8,9,10. Nucl. Phys. A **745**(3), 155–362 (2004). https://doi.org/10.1016/j.nuclphysa.2004.09.059. http://www.sciencedirect.com/science/article/pii/S0375947404010267
36. W. Elkamhawy, H.-W. Hammer, in preparation (2019)
37. V. Lensky, M.C. Birse, Coupled-channel effective field theory and proton-^{7}Li scattering. Eur. Phys. J. A **47**, 142 (2011). https://doi.org/10.1140/epja/i2011-11142-0. arXiv:1109.2797
38. E. Ryberg, C. Forssén, H.-W. Hammer, L. Platter, Effective field theory for proton halo nuclei. Phys. Rev. C **89**, 014325 (2014). arXiv:1308.5975
39. E. Ryberg, C. Forssén, H.-W. Hammer, L. Platter, Constraining Low-Energy Proton Capture on Beryllium-7 through Charge Radius Measurements. Eur. Phys. J. A **50**, 170 (2014). https://doi.org/10.1140/epja/i2014-14170-2. arXiv:1406.6908
40. X. Zhang, K.M. Nollett, D.R. Phillips, Halo effective field theory constrains the solar $^{7}\mathrm{Be} + \mathrm{p} \rightarrow {}^{8}\mathrm{B} + \gamma$ rate. Phys. Lett. B **751**, 535–540 (2015). https://doi.org/10.1016/j.physletb.2015.11.005. arXiv:1507.07239
41. E. Ryberg, C. Forssén, H.-W. Hammer, L. Platter, Range corrections in Proton Halo Nuclei. Ann. Phys. **367**, 13–32 (2016). https://doi.org/10.1016/j.aop.2016.01.008. arXiv:1507.08675
42. C.H. Schmickler, H.-W. Hammer, A.G. Volosniev, Universal physics of bound states of a few charged particles. Phys. Lett. B **798**, 135016 (2019). https://doi.org/10.1016/j.physletb.2019.135016. arXiv:1904.00913
43. D.R. Tilley, H.R. Weller, C.M. Cheves, Energy levels of light nuclei A = 16–17. Nucl. Phys. A **564**, 1–183 (1993). https://doi.org/10.1016/0375-9474(93)90073-7
44. D.R. Tilley, C.M. Cheves, J.L. Godwin, G.M. Hale, H.M. Hofmann, J.H. Kelley, C.G. Sheu, H.R. Weller, Energy levels of light nuclei A=5, A=6, A=7. Nucl. Phys. A **708**, 3–163 (2002). https://doi.org/10.1016/S0375-9474(02)00597-3
45. K.M. Nollett, R.B. Wiringa, Asymptotic normalization coefficients from ab initio calculations. Phys. Rev. C **83**, 041001 (2011). https://doi.org/10.1103/PhysRevC.83.041001